



Article

Turbulence Parameters in the Troposphere—Lower Stratosphere Observed by Beijing MST Radar

Ze Chen ^{1,2,3} , Yufang Tian ^{1,2,3,*} and Daren Lü ^{1,2,3}

- ¹ Key Laboratory of Middle Atmosphere and Global Environment Observation (LAGEO), Institute of Atmospheric Physics, Chinese Academy of Sciences, Beijing 100029, China; chenze@mail.iap.ac.cn (Z.C.); ludr@iap.ac.cn (D.L.)
- ² Xianghe Observatory of Whole Atmosphere, Institute of Atmospheric Physics, Chinese Academy of Sciences, Xianghe, Langfang 065400, China
- ³ University of Chinese Academy of Sciences, Beijing 100049, China
- * Correspondence: tianyufang@mail.iap.ac.cn

Abstract: Based on three years of data observed by Beijing MST radar between 2012 and 2014, this study gives the distribution characteristics of the turbulence energy dissipation rate ϵ and the vertical turbulence diffusion coefficient K_z in the troposphere–lower stratosphere over Beijing based on the spectral width method. Additionally, from the perspective of atmospheric stability expressed by the Brunt–Väisälä frequency N and the gradient Richardson number Ri , the seasonal variations of turbulence parameters at different heights are analyzed. The results show that ϵ (K_z) is distributed in the range of 10^{-4} to $10^{-1.5}$ $\text{m}^2 \text{s}^{-3}$ (10^0 to 10^1 $\text{m}^2 \text{s}^{-1}$), with median values of 10^{-3} to $10^{-2.5}$ $\text{m}^2 \text{s}^{-3}$ ($10^{0.4}$ to $10^{0.75}$ $\text{m}^2 \text{s}^{-1}$). In the height range of -1 km to about $+1$ km from the tropopause, the profiles of ϵ have no noticeable seasonal difference from October to next May, and ϵ increases sharply with the slope of linear regression $\nabla \log(\epsilon)/\nabla h = 0.25$ ($\text{m}^2 \text{s}^{-3}$) km^{-1} . The seasonal variation of turbulence parameters has noticeable differences at different atmospheric layers. Furthermore, the atmospheric static/dynamic stability and turbulence intensity are the influencing factors of turbulence parameters. From the tropopause to 14 km, the values of ϵ and N both have a peak from October to next May, and this peak layer disappears from July to August. Within the range of 2–4 km from the ground, K_z and the frequency of $Ri < 0.25$ have a significant positive correlation, with a Pearson correlation coefficient greater than 0.5, and both have large value layers in March to May and September to October. The turbulence intensity above 15 km is likely the main factor affecting the turbulence dissipation rate and vertical turbulence diffusion coefficient.

Keywords: turbulence energy dissipation rate; vertical eddy diffusion coefficient; atmospheric stability; Beijing MST radar



Citation: Chen, Z.; Tian, Y.; Lü, D. Turbulence Parameters in the Troposphere—Lower Stratosphere Observed by Beijing MST Radar. *Remote Sens.* **2022**, *14*, 947. <https://doi.org/10.3390/rs14040947>

Academic Editor: Maria João Costa

Received: 28 December 2021

Accepted: 11 February 2022

Published: 15 February 2022

Publisher's Note: MDPI stays neutral with regard to jurisdictional claims in published maps and institutional affiliations.



Copyright: © 2022 by the authors. Licensee MDPI, Basel, Switzerland. This article is an open access article distributed under the terms and conditions of the Creative Commons Attribution (CC BY) license (<https://creativecommons.org/licenses/by/4.0/>).

1. Introduction

Small-scale turbulence plays an essential role in the vertical exchange of heat, momentum, and matter in the atmosphere. Atmospheric turbulence not only occurs in the planetary boundary layer but also at other altitudes, such as the statically stable stratosphere. Understanding the intensity and other parameters of turbulence is essential in numerical weather prediction and atmospheric chemistry simulation, as well as for an in-depth understanding of atmospheric dynamics. In terms of turbulence observations in the free atmosphere, early in-situ observations were mainly carried out by radiosonde balloons and airplanes [1]. However, since then, with the development of atmospheric radar, it is now possible to quantitatively calculate turbulence parameters of the free atmosphere (such as the turbulence energy dissipation rate ϵ and the vertical eddy diffusion coefficient K_z) through remote sensing [2,3].

The atmospheric radar echo signal contains turbulence information. Most current research on radar-based turbulent parameters is based on the Kolmogorov assumption of

isotropic turbulence in the inertial range [4–6]. Due to the distribution characteristics of turbulence scale at each height [4], atmospheric radar needs to select different wavebands to detect isotropic Kolmogorov turbulence at different heights. For MST radar, electromagnetic wave in VHF band should be selected. The Beijing MST radar emits electromagnetic waves with a wavelength of 6 m, thus it can be assumed that the turbulence considered in this paper (troposphere–lower stratosphere) is indeed isotropic Kolmogorov turbulence.

To be able to use atmospheric radar to detect the intensity of atmospheric turbulence, the radar echo signal should come from turbulence scattering. However, in reality, radar is often affected by specular reflection, and the oblique beam is less affected by specular reflection than the vertical beam. Mesosphere–stratosphere–troposphere (MST) radar is an atmospheric radar with the ability to detect turbulence characteristics in multiple layers of the atmosphere. Therefore, MST radar is a unique and vital means of detecting free atmospheric turbulence.

Atmospheric radar is a type of Doppler radar. The spectral width of the radar contains information on the intensity of atmospheric turbulence, and the scale of atmospheric turbulence detected by the radar is smaller than the radar sampling volume. Hocking [4] and Nastrom [7] pointed out that broadening the radar signal spectrum is mainly affected by turbulence and non-turbulence. Non-turbulent factors of influence include the beam width, wind shear, and gravity waves. Using turbulence spectral width data can allow parameters such as the turbulence dissipation rate, vertical turbulence dissipation coefficient, turbulence inner scale, turbulence outer scale, and radar reflection cross section to be estimated. Such a method is called the spectral width method. At present, there are mainly three models used to calculate the non-turbulent spectral width: the calculation models proposed by Hocking [3,4], Nastrom [7], and Dehghan and Hocking [8], respectively. In addition to the spectral width method, other methods can also calculate turbulence parameters, including the power method [7] and the vertical velocity variance method [9].

Some studies have used the Thorpe method [10] to calculate atmospheric turbulence parameters based on radiosonde data and compared radar-based and radiosonde-based turbulence parameter statistical results in the troposphere–lower stratosphere. Previous studies have shown that the turbulence parameters calculated using MST radar data are in good agreement with the calculated results using radiosonde data [11–13]. Kantha and Hocking [13] and Li et al. [14] compared the ε calculated by radar data and radiosonde data. They used the radar datasets of Harrow VHF (very high frequency) radar (42.04° N, 82.89° W) and MAARSY (Middle Atmosphere Alomar Radar System) radar (69.03° N, 16.04° E), respectively. Their results both showed that the radar-based ε was in good agreement with the radiosonde-based ε in the range of values, median values, and frequency distribution. Kohma et al. [13], using the PANSY (Program of the Antarctic Syowa Mesosphere–Stratosphere–Troposphere/Incoherent Scatter) radar at Syowa Station (69.00° S, 39.35° E), calculated atmospheric turbulence parameters (1.5–19 km) on the Antarctic continent from October 2015 to September 2016 and compared the turbulent parameters with the results of radiosonde data. The results showed that the consistency between the radar-based and radiosonde-based ε changes with altitude was better. Nonetheless, the radiosonde-based results were two to five times larger than the radar-based results. The authors pointed out that this may have been because, for deep overturning layers, sounding data will overestimate the value of ε when the Thorpe method is used to estimate it.

In the Antarctic, Arctic, midlatitudes, and low latitudes, some studies have used radar data to study the characteristics of turbulence parameters in the troposphere–lower stratosphere. For example, the profile characteristics of turbulence parameters vary with height from the ground/tropopause, as well as their daily, seasonal, and interannual variations. Table 1 shows statistical results of turbulence parameters derived from MST and ST radars in the troposphere–lower stratosphere in different latitudes (a total of 10 radars), revealing that there are specific differences in the statistical results of turbulence parameters across different studies. Jaiswal et al. [14] pointed out that the turbulence parameters of

the central Himalayas with its complex topography are an order of magnitude higher than those of southern India.

Table 1. Turbulence parameters in the troposphere–lower stratosphere from different radars.

Station	Altitude (Range Resolution)	Turbulence Parameter	Citation
PANSY (69.00° S, 39.35° E)	1.5–19 km (150 m)	$\log(\epsilon)$ -5 to -3 $\text{m}^2 \text{s}^{-3}$	Khoma et al., 2019 [13]
MARRSY (69.03° N, 16.04° E)	5–17 km (300 m)	$\log(\epsilon)$: -7 to -2 $\text{m}^2 \text{s}^{-3}$ median ϵ 1.13×10^{-4} to 2.50×10^{-4} $\text{m}^2 \text{s}^{-3}$	Li et al., 2016 [12]
Harrow (42.04° N, 82.89° W)	1.5–11 km (500 m)	$\log(\epsilon)$: -4 ~ -2 $\text{m}^2 \text{s}^{-3}$	Kantha and Hocking 2011 [15]
MU (35° N, 136° E)	Troposphere 5–20 km (150 m)	$\log(K_z)$ 0 $\text{m}^2 \text{s}^{-1}$ $\log(K_z)$ -0.7 to 0.3 $\text{m}^2 \text{s}^{-1}$	Fukao et al., 1994 [16] Yamanaka et al., 1994, Kurosaki et al., 1996 [17,18]
VBG (34°46'48" N, 120°33'36" W)	2–21 km (150 m)	median $\log(\epsilon)$: -3.7 (8 km) to -3.1 $\text{m}^2 \text{s}^{-3}$ (2/21 km)	Nastrom and Eaton 2005 [19]
WSMR (32° N, 106° W)	5–20 km (150 m)	median/mean $\log(\epsilon)$: -3.5 to -2.5 $\text{m}^2 \text{s}^{-3}$	Nastrom and Eaton 1997 [20,21]
ARIES ST (28.4° N, 79.5° E)	3–12 km (150 m)	mean $\log(\epsilon)$: -3 to -2 $\text{m}^2 \text{s}^{-3}$	Jaiswal et al., 2020 [14]
Gadanki (13.5° N, 79.2° E)	7.5–21 km (150 m)	median $\log(\epsilon)$: -4 to -3 $\text{m}^2 \text{s}^{-3}$	Rao et al., 2001 [22,23]
Tirupati (13.47° N, 79.1° E)	4–19 km (150 m)	$\log(\epsilon)$: -6 to -3 $\text{m}^2 \text{s}^{-3}$	Rao et al., 1997 [24]
Pune (UHF) (18°32' N, 73°51' E)	1.05–10.35 km (300 m)	mean $\log(\epsilon)$: -6.4 to -3 $\text{m}^2 \text{s}^{-3}$	Singh et al., 2008 [25]

To date, relevant research on using MST radar data to analyze the interannual, seasonal, and diurnal variation characteristics of turbulence parameters at different heights has been limited to just a few regions. The study of the vertical distribution of turbulence parameters and their changes plays an essential role in understanding the formation and development of clouds and precipitation, the coupling between atmospheric regions (troposphere-stratosphere exchange), and the coupling of dynamic processes at different scales in the atmosphere (gravity wave breaking produces turbulence, which in turn affects atmospheric dynamics and thermal distribution characteristics). In this sense, MST radar can also support measured data related to the distribution and change of turbulence parameters for weather and climate forecasting models.

Due to the importance of this kind of research, this study uses the spectral width method to calculate the ϵ and K_z . Section 2 describes the data and methods used in this study. Section 3 analyzes the seasonal and annual mean vertical distribution characteristics of each turbulence parameter. Section 4 compares the seasonal variation characteristics of atmospheric turbulence parameters and atmospheric static/dynamic stability. Conclusions are given in Section 5.

2. Data and Methods

2.1. Data

2.1.1. Beijing MST Radar

The data used in this paper are the observational data of Beijing MST radar, which is located at the Xianghe Observatory of the Whole Atmosphere, Institute of Atmospheric Physics, Chinese Academy of Sciences (39.78° N, 116.95° E). Beijing MST radar was built and put into operation in 2011 and has since accumulated a long period of data. According to analyses of the reliability and accuracy of Beijing MST radar data [26,27], it has good detection capability in the troposphere, lower stratosphere, and mesosphere to lower thermosphere.

When the radar is working normally, there are three observation modes: high, medium, and low. Each observation mode uses five beams (east, west, south, north, and vertical). This study uses the oblique beam (east-west, north-south) data in the medium observation mode. The radial range resolution of the radar is 600 m, and the parameters of the radar are

listed in Table 2. For a more detailed description, refer to Tian and Lü [28]. Before using the radar observation data, an improved processing algorithm of power spectral density [28] was applied, which can effectively suppress non-atmospheric signals and obtain reliable spectral width data.

Table 2. Parameters of the medium observation mode of Beijing MST radar.

Parameter	Value
Location	Xianghe Station, China (39.78° N, 116.95° E)
Operating frequency	50 ± 1 MHz
Number of beams	5 (E, W, S, N, V)
Peak power output	172.8 kW
Half-power full-beam width	3°
Zenith angle of oblique	15°
Coherent integration	64
Incoherent integration	10
Number of FFT	256
Pulse length	32 μs
Interpulse period	320 μs
Range resolution	600 m

When using radar spectral width data to calculate turbulence parameters, the advantage of using vertical beam detection is that it does not need to consider the effects of wind shear [29]. However, vertical beams are more susceptible to specular reflections, such as a static stability tropopause. Compared with vertical beams, oblique beams are less likely to be affected by specular reflection than the isotropic scattering of isotropic turbulence [16,30]. Therefore, this paper uses the spectral width data from four oblique beams to calculate the turbulence parameters.

2.1.2. Radiosonde Data

When using the spectral width method to calculate radar-based turbulence parameters through the turbulence spectral width data, other datasets are needed to provide the profile of Brunt–Väisälä (B–V) frequency N . This study uses the temperature profile data of conventional radiosondes in Beijing (54,511; 39.8° N, 116.4° E) to calculate N^2 ,

$$N^2 = g \frac{\partial \ln \theta}{\partial z},$$

where g is the acceleration of gravity and θ is potential temperature. The straight-line distance between the sounding launch site and the MST radar station is about 40 km. It is assumed that the N obtained from the radiosonde is suitable for the Beijing MST radar station. Conventional radiosondes carry out detections twice a day. The sounding balloon release time is 1115 and 2315 (UTC) with a record every 1–2 s, and the vertical resolution is about 10 m. The medium observation mode of Beijing MST radar makes an observation every half an hour. The times of the selected radar observation data are 1110, 1140, 2310, and 2340 (UTC).

From 2012 to 2014, there were a total of 3532 profiles of radar observational data (corresponding to 1766 radiosonde profiles) involved in the calculation of turbulence parameters. For convenience of analysis, when using the radar observational data to calculate the turbulence parameters, the radiosonde data are interpolated with a resolution of 600 m.

2.2. Methods

Radar echo is the backscattering result of all scattering cells in the radar sampling space. For a given range bin, due to coherent integration and incoherent integration of the radar, the random motion of the scattering cells is shown as the random distribution of its Doppler velocity near the mean wind speed. That is, the Doppler spectrum of the radar is broadened. The Doppler spectral width contains atmospheric turbulence information and can be used to calculate the parameters of turbulence.

The main factors contributing to the measured spectral width σ_o^2 of the MST radar include turbulence σ_t^2 , radar beam broadening (beam width, tilt angle), horizontal wind shear $\sigma_{s\&b}^2$, and gravity waves σ_w^2 . In the troposphere–lower stratosphere region, the influence of gravity waves on the observed spectrum width is relatively small compared to the other two. The specific formula of each contributing item is

$$\sigma_o^2 = \sigma_t^2 + \sigma_{s\&b}^2 + \sigma_w^2. \quad (1)$$

For non-turbulent flow leading to broadening of the spectrum, Dehghan and Hocking [8] gave a new calculation model (referred to as the D–H model) based on the 2D model proposed by Nastrom [7]. The new model has one more item than the original 2D model, and Dehghan and Hocking [8] considered that the result of the D–H model is more accurate than the N-2D model. The formula is as follows:

$$\begin{aligned} \sigma_{s\&b}^2 = & \frac{\theta^2}{k} v^2 \cos^2 \chi - a_0 \frac{\theta}{k} \sin \chi \left(v \frac{\partial v}{\partial z} \zeta \right) + b_0 \frac{2 \sin^2 \chi}{8k} \left(\frac{\partial v}{\partial z} \zeta \right)^2 \\ & + c_0 \left(\cos^2 \chi \sin^2 \chi \right) |v \zeta| + d_0 \left(\cos^2 \chi \sin^2 \chi \right) \zeta^2, \end{aligned} \quad (2)$$

where $k = 4 \ln 2$, $\zeta = 2r\theta \sin \chi$, $\xi = \frac{\partial v}{\partial z} \Delta r$, $a_0 = 0.945$, $b_0 = 1.500$, $c_0 = 0.030$, $d_0 = 0.825$, θ is the half-power and half-width, v is the horizontal wind speed, $\partial v / \partial z$ is the vertical shear of horizontal wind speed, χ is the zenith angle of the radar beam, r is the distance, and Δr is the radar resolution.

When using the spectral width method, there will be cases of negative σ_t^2 , referred to as negative turbulent kinetic energy (N-TKE), which has no actual physical meaning. Dehghan and Hocking [9] suggested that the main factors that cause a negative value of the turbulent spectrum width are the non-isotropy of the scatterer (the contribution is relatively small), the uncertainty of the calculations of observational spectral width, and the spectral width broadening term Equation (1).

Figure 1 shows the percentage distribution of N-TKE at various heights from 2012 to 2014, during which period there were no observational data in September of 2013 and 2014. In winter, the proportion of N-TKE at 5–9 km is significantly higher than that in other regions, but the maximum percentage of N-TKE is less than 5%. Therefore, from the perspective of the occurrence rate of N-TKE, the statistical results in this paper are credible.

Assuming that the turbulence in the inertial subregion is isotropic, for a stably stratified atmosphere, the turbulence spectral width σ_t^2 and the ε have the following relationship [2]:

$$\varepsilon = A^{-3/2} N \sigma_t^2 \quad (3)$$

where A is the Kolmogorov constant, taking $A = 1.6$ and N is the buoyancy frequency (B-V frequency), calculated from Beijing radiosonde data.

The vertical turbulent dissipation coefficient K_z is closely related to the turbulent dissipation rate ε [7,16,22], and the formula is as follows:

$$K_z = 0.3 \varepsilon N^{-2} = 0.15 N^{-1} \sigma_t^2 \quad (4)$$

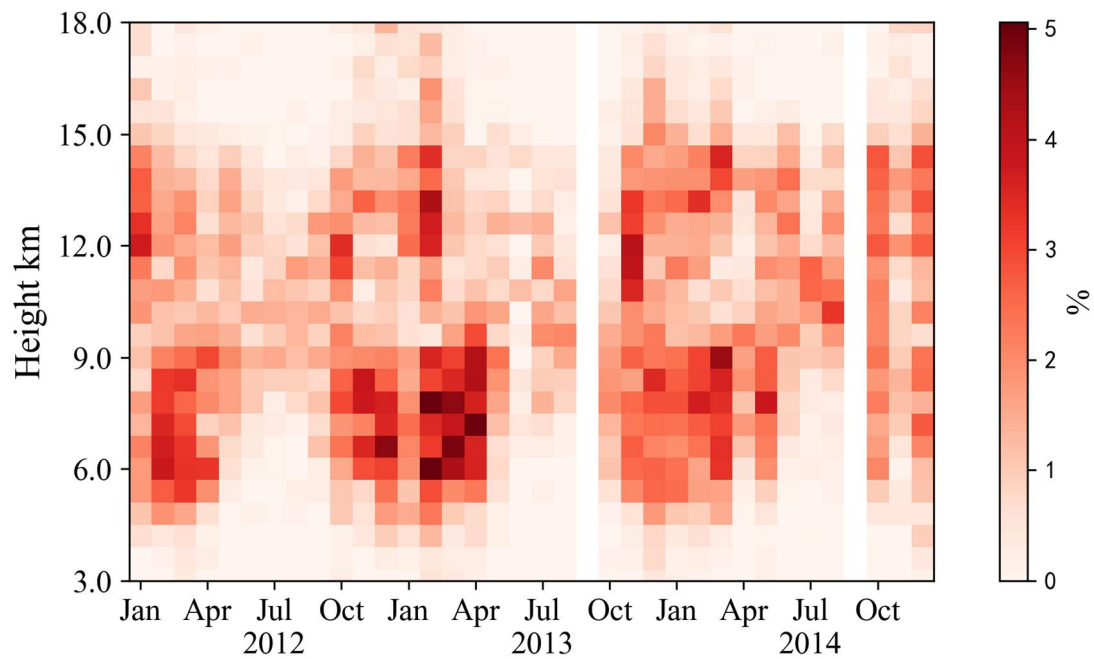


Figure 1. Monthly N-TKE frequency for each altitude from 2012 to 2014. There were no data for September 2013 and 2014.

3. Results

3.1. Statistical Characteristics of Turbulence Parameters

Figure 2 shows the distribution and median profile of the logarithmic value of ε in every 3-km range from 3 to 18 km, as well as the upper and lower quartile profiles. ε is distributed from 10^{-4} to $10^{-1.5}$ $\text{m}^2 \text{s}^{-3}$, spanning 2.5 orders of magnitude, and the shape conforms to the Gaussian distribution. The median distribution of ε is from 10^{-3} to $10^{-2.5}$ $\text{m}^2 \text{s}^{-3}$, and the upper and lower quartiles of $\log(\varepsilon)$ are approximately between the median values ± 0.25 . ε decreases from $10^{-2.6}$ $\text{m}^2 \text{s}^{-3}$ at 3 km to 10^{-3} $\text{m}^2 \text{s}^{-3}$ at 7.5 km, and increases from 7.5 km to $10^{-2.2}$ $\text{m}^2 \text{s}^{-3}$ at 18 km. The increasing rate of ε from 7.5 to 11 km is significantly greater than the increasing rate of the height region above 11 km.

Figure 3 shows the distribution of K_z logarithmic values and the median profile and the upper and lower quartile profiles in the range of 3–18 km every 3 km. The K_z distribution is from 10^0 to 10^1 $\text{m}^2 \text{s}^{-1}$, spanning an order of magnitude, and the shape conforms to the Gaussian distribution. The median of K_z is distributed from 10^4 to $10^{0.75}$ $\text{m}^2 \text{s}^{-1}$, and the upper and lower quartiles of $\log(K_z)$ are approximately between the median values ± 0.25 . K_z decreases from $10^{0.75}$ $\text{m}^2 \text{s}^{-1}$ at 3 km to $10^{0.5}$ $\text{m}^2 \text{s}^{-1}$ at 10 km. From 10 to 18 km, K_z changes very little with height, and the value is about $10^{0.5}$ $\text{m}^2 \text{s}^{-1}$.

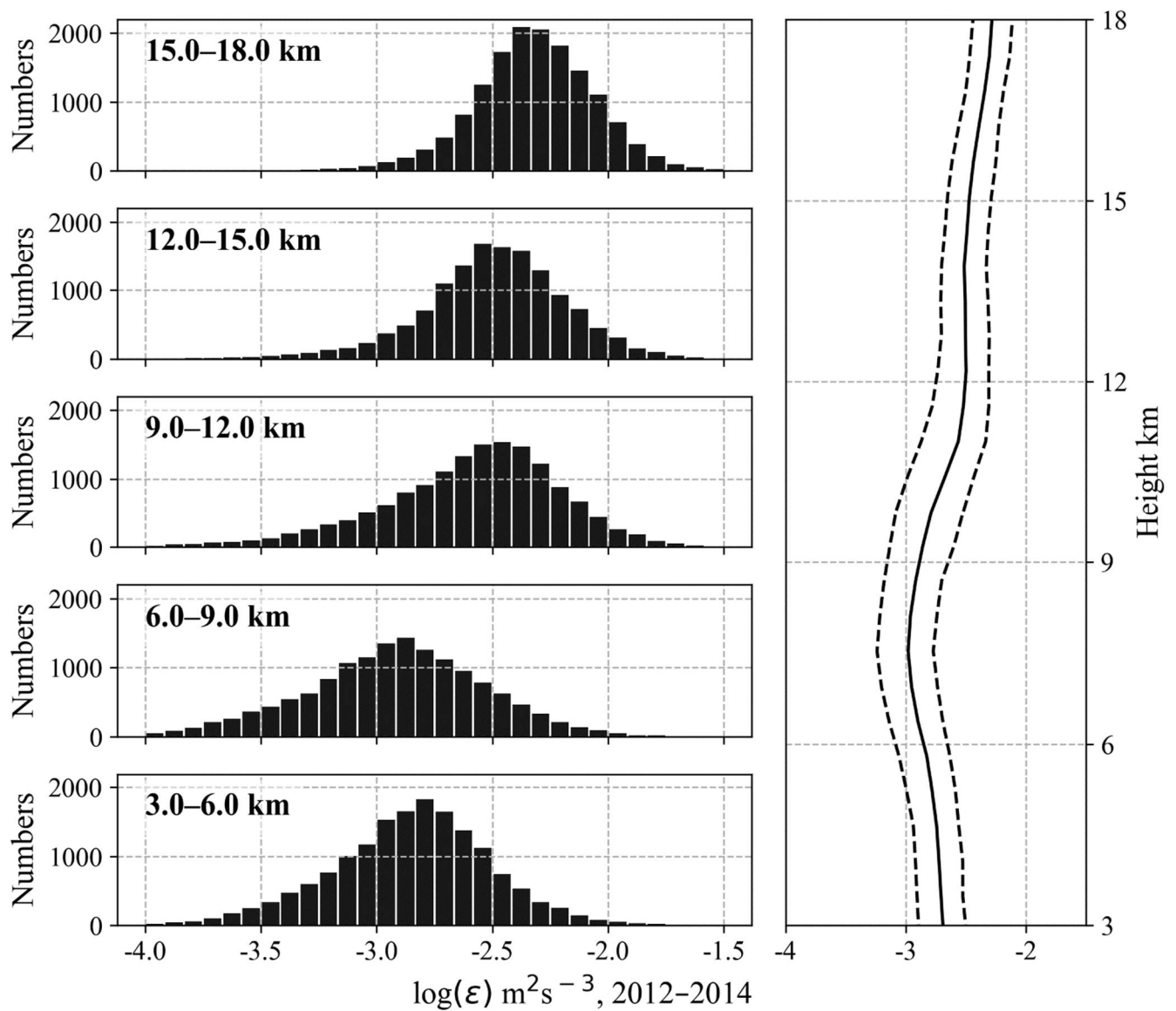


Figure 2. The histograms on the left present the frequency distribution of the logarithmic value of the turbulent energy dissipation rate ϵ in every 3 km range within 3–18 km. The subplots on the right show the median and upper and lower quartile profiles of $\log(\epsilon)$.

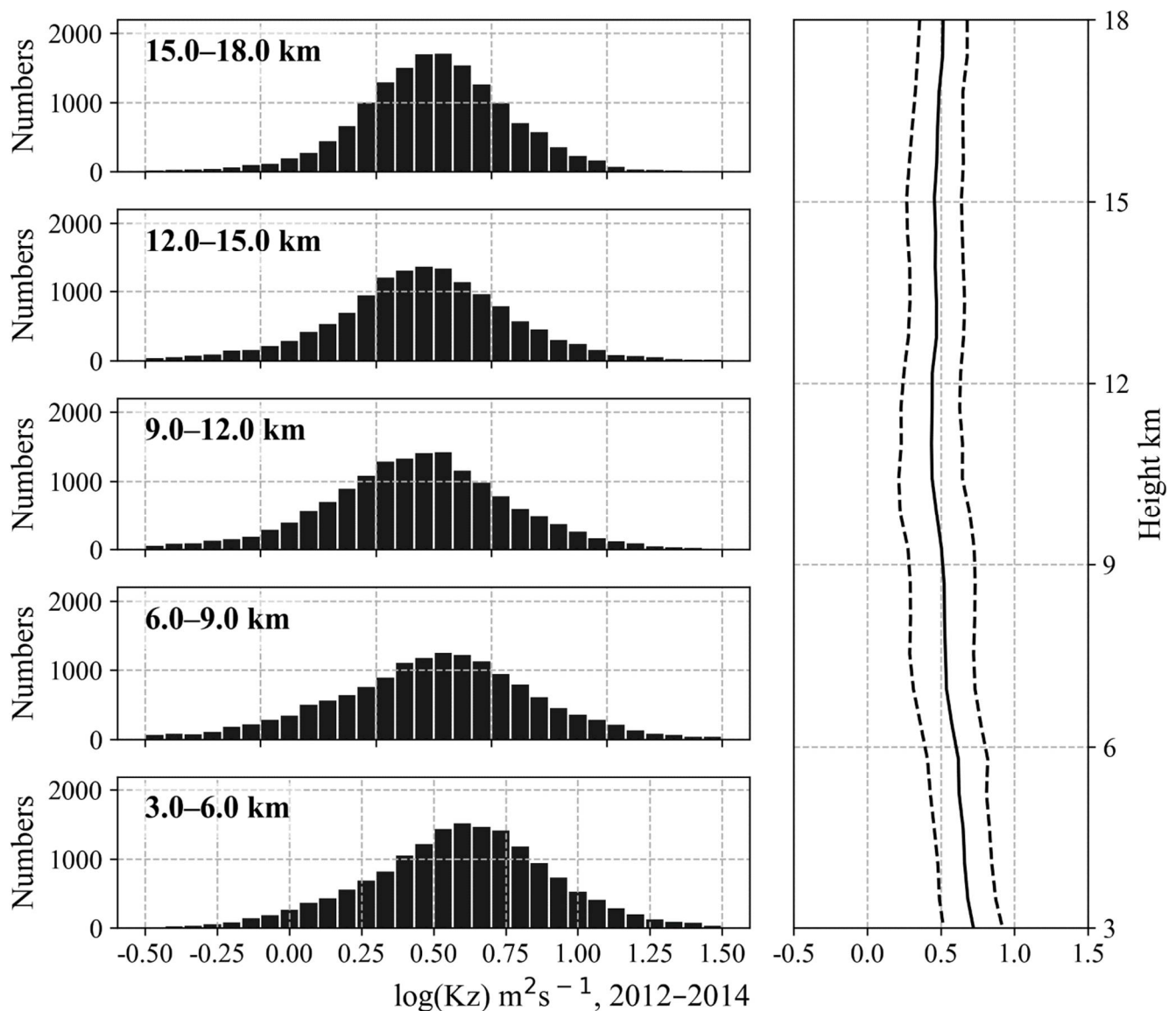


Figure 3. The histograms on the left present the frequency distribution of the logarithmic value of the vertical turbulence diffusion coefficient K_z in every 3-km range within 3–18 km. The subplots on the right show the median and upper and lower quartile profiles of $\log(K_z)$.

3.2. Seasonal Variation of Turbulence Parameters with Height from the Ground

This section uses the Beijing MST radar observational data from 2012 to 2014 to analyze the variational characteristics of turbulence parameters in each month with height from the ground.

The value of ε in the stratosphere is higher than in the troposphere, as shown in Figure 4a. The median value of ε in each month is distributed from $10^{-3.2}$ to $10^{-2.1} \text{ m}^2 \text{ s}^{-3}$. There is a minimum value of ε in the troposphere. The contours clearly show that the lower boundary of the small-value layer has no apparent monthly difference, while the upper boundary increases (decreases) with the increase (decrease) in the tropopause height. The tropopause height is about 15 km in July and August, and the lowest height of the tropopause is about 9 km in December and January. Furthermore, the center position of this minimum layer is about 7.5 km from October to the following May, and the height is about 10 km in July and August. June and September are more likely the transitional months.

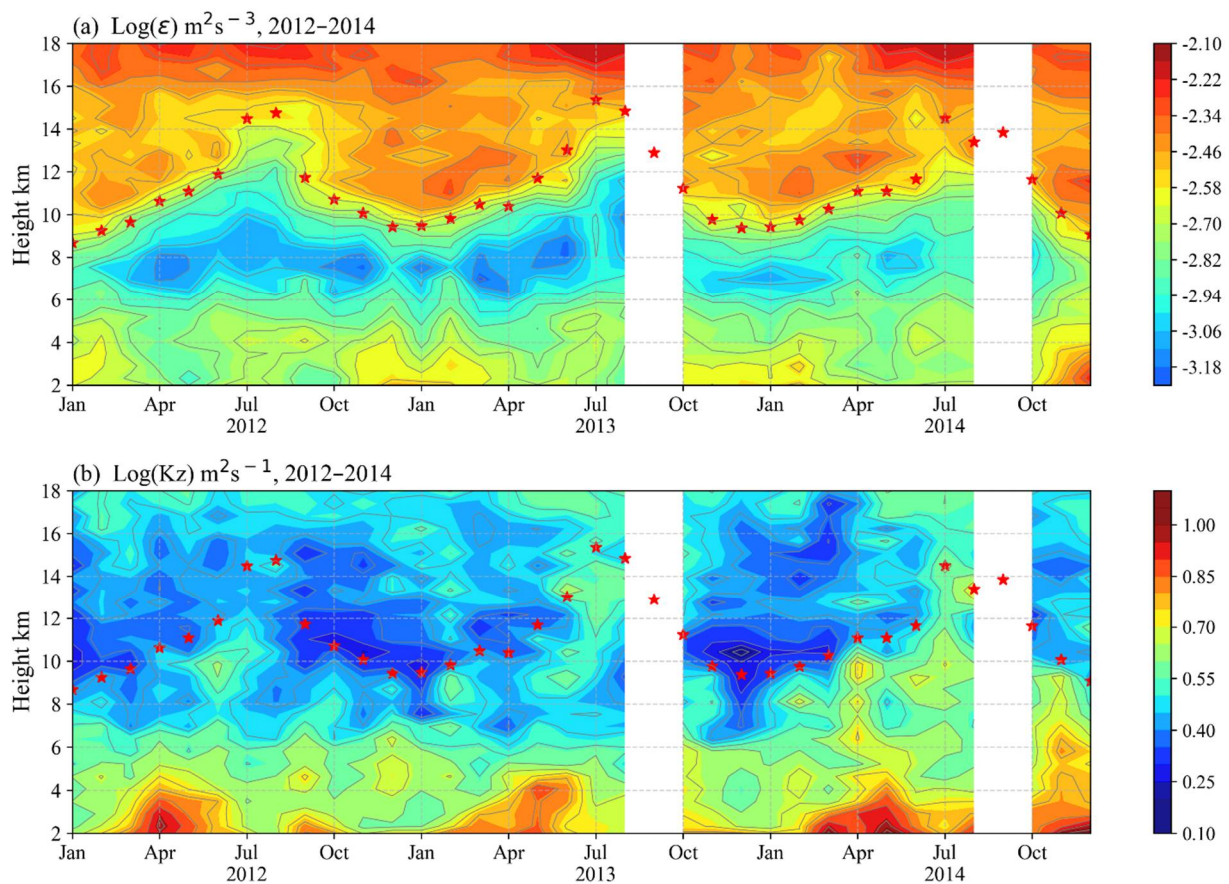


Figure 4. Monthly median values of (a) $\log(\epsilon)$ and (b) $\log(K_z)$ as a function of height in Beijing from 2012 to 2014. The stars are the monthly averaged thermal lapse-rate tropopause heights from radiosonde data.

In the height region below 7.5 km, below the minimum value of ϵ , ϵ decreases with height from the ground in each month. Additionally, the density of the contours indicates that the rate of decline of ϵ has no obvious monthly difference in the height region below 7.5 km. The highest increasing rate is at a few kilometers above and below the tropopause. However, the density of the contours in July and August is weaker than in other months, which shows that the increasing rate in the tropopause in July and August is lower than in other months.

In the range from the tropopause to 14 km, the value of ϵ has a peak layer from October to the following May. The peak layer starts in September and disappears in June of the following year. In July and August in Beijing, this layer disappears due to the tropopause rising to over 14 km. In the range of 15–18 km in Beijing, the value of ϵ from May to October is significantly larger than in other months.

The K_z of the troposphere is greater than the value of the stratosphere and has a rougher profile in each month compared with ϵ , as shown in Figure 4b. The median value of K_z in each month is distributed between $10^{0.1}$ and $10^{1.0} \text{ m}^2 \text{ s}^{-1}$. In the range of 2–4 km from the ground, there is a large value from March to May and from September to October. Additionally, the value is larger and the thickness of this large-value layer is thicker from March to May.

At 1 km above the tropopause, K_z has a minimum value in each month except July and August, and the distance from the ground is about 11 km. In July and August, the tropopause rises and this minimum layer disappears. At the height of several kilometers below the tropopause, there is an extreme-value zone for K_z , and the height of the large-value zone rises as the tropopause height rises, which leads to K_z having no minimum

zone around 10–11 km in July and August. The upper boundary of the range in the decline in height of K_z in the troposphere is about 7.5 km in July and August. However, this upper boundary is at 1 km above the tropopause (the height of the minimum K_z value) in other months. Therefore, in July and August, in the height range from 7.5 km to 15 km, the characteristics of K_z changing with height are different from the other months.

The monthly variations in the vertical structure of K_z indicate that in the mid–lower troposphere and the region around the tropopause, there are apparent differences in the variation. When discussing the seasonal variation characteristics of the vertical structure of K_z , it is necessary to consider the suitability of seasonal divisions in different atmospheric layers.

4. Discussion

4.1. Comparison of Atmospheric Turbulence Parameters and Atmospheric Stability

Unstable airflow will become or maintain turbulent flow and stable airflow will become or maintain laminar flow. This section analyzes the seasonal changes of turbulence parameters in the troposphere–lower stratosphere over Beijing from the perspective of atmospheric stability. Many factors determine the atmospheric stability, and these influencing factors can be understood as items in the turbulent kinetic energy (TKE) budget equation. There is static stability that is a measure of buoyancy convection capacity, and the BV frequency can represent the static stability of the atmosphere. Static means no movement. That is, the static stability does not consider the influence of wind. However, there is wind shear in the actual atmosphere, and even if the atmosphere is stable, wind shear can produce mechanical turbulence. When considering the terms of the TKE budget equation, to effectively approximate the simplification, researchers define the dimensionless ratio of the buoyancy generation term and the mechanical generation term as the flux Richardson number R_f .

The R_f includes turbulence-related factors. We can only use R_f to determine whether the turbulent flow can become a laminar flow, but we cannot judge whether the laminar flow can become turbulent. According to K theory, the gradient is directly proportional to the turbulence correlation. Therefore, if the gradient replaces the turbulence correlation in R_f , a new ratio can be obtained, called the gradient Richardson number R_i . The formula is as follows:

$$R_i = \frac{\frac{g}{\theta_v} \frac{\partial \overline{\theta_v}}{\partial z}}{(\frac{\partial \overline{U}}{\partial z})^2 + (\frac{\partial \overline{V}}{\partial z})^2} = \frac{N^2}{(\frac{\partial \overline{U}}{\partial z})^2 + (\frac{\partial \overline{V}}{\partial z})^2} \quad (5)$$

where g is the gravitational acceleration, θ_v is the potential temperature, and $(\frac{\partial \overline{U}}{\partial z})^2 + (\frac{\partial \overline{V}}{\partial z})^2$ is the square value of the horizontal wind vertical shear. The B-V frequency can be calculated using the formula $N^2 = \frac{g}{\theta_v} \frac{\partial \overline{\theta_v}}{\partial z}$.

When $R_f > 1$, the buoyancy term is greater than the mechanical term, and the atmosphere will maintain or become a stable laminar flow. When $R_f < 1$, the atmosphere is considered unstable, and the atmosphere maintains or becomes turbulent. However, for R_i , when $R_i < R_d$, the atmosphere is unstable, and when $R_i > R_t$ the atmosphere is considered stable. The value of R_t is 1, and the value of R_d is in the range of 0.22–0.25. This paper takes $R_d = 0.25$.

Based on the observational data of Beijing MST radar from 2012 to 2014, this section compares the median logarithmic values of turbulence parameters with the values of the atmospheric stability in each month. The atmospheric stabilities used in this study include atmospheric static stability, B-V frequency N , atmospheric dynamic stability, and gradient Richardson number R_i . Figure 5 shows the monthly median values of B-V and the percentage of $R_i < 0.25$ at each height from 2 to 18 km.

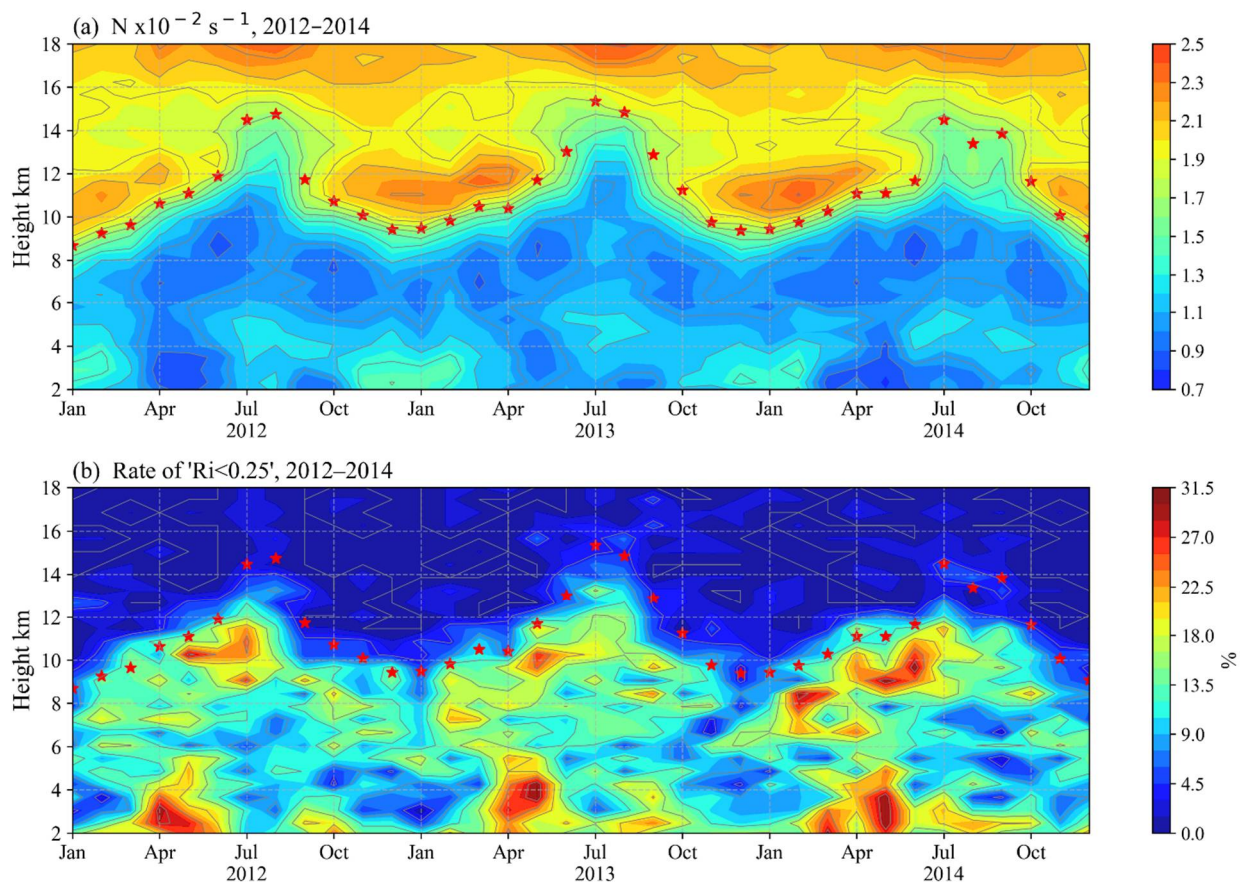


Figure 5. Monthly median values of (a) N and (b) percentage of $Ri < 0.25$ as a function of height in Beijing from 2012 to 2014. The stars are the monthly averaged thermal lapse-rate tropopause heights obtained based on radiosonde data.

In the height region of 2–18 km in Beijing, the seasonal variation characteristics of ε and N are in good agreement. Section 3.2 shows that from the tropopause to 16 km, there is an apparent large-value layer for ε from October to the following May. June and September are the transition months for this high-value layer. The values of N also have the same seasonal characteristics, as shown in Figure 5a. From October to the following May, the contours of ε are very dense at the tropopause. N also has the same characteristics at the tropopause, which shows that the large gradient of ε at the tropopause is related to N . The values of ε and N have a corresponding excellent relationship between the large values and the small values. Function (3) also shows that ε has a positive correlation with N and turbulence intensity. However, this section mainly compares the seasonal characteristics of Beijing's turbulence parameters and atmospheric stability at mid-high latitudes.

In the height region below the tropopause in Beijing, K_z has a corresponding good relationship with the large values of the percentage of $Ri < 0.25$. Within the range of 2–4 km, the percentage of $Ri < 0.25$ and the values of K_z both have a large-value layer from March to May and from September to October. From March to May, the percentage of $Ri < 0.25$ is greater than in September and October, and the upper boundary of this large value layer is significantly higher than from September and October. In the height region of 2–3 km below the tropopause, the large value of the percentage of $Ri < 0.25$ corresponds to the large value of K_z .

This study also finds that the seasonal variation of atmospheric turbulence parameters has significant differences in different atmospheric layers. When considering the beginning and end months of a season, the division points of different layers might be different. For example, the values of ε and N have noticeable seasonal changes from the tropopause

to 16 km in Beijing. However, the values have no obvious seasonal variation in some height ranges, mainly in the range of 6–8 km and the heights below 6 km. For K_z and the percentage of $Ri < 0.25$, the values have different seasonal variation in different atmospheric layers—mainly the heights below 4 km and the range from 8 km to the tropopause. These characteristics show that even when studying the seasonal characteristics of atmospheric turbulence parameters at different levels at the same station, it is necessary to pay attention to the difference between the beginning and end months of different seasons. This section mainly discusses and compares the seasonal characteristics of atmospheric turbulence parameters and atmospheric stability in mid-high latitude regions, but the causes of these characteristics need to be further investigated.

4.2. Correlation Analysis of Turbulence Parameters and Atmospheric Stability/Turbulence Intensity

Section 4.1 shows that the turbulence parameters and the atmospheric static/dynamic stability have a good relationship at some altitudes. At the same time, the turbulence intensity (turbulence spectrum width σ_t^2) is also one of factors influencing turbulence parameters (Formulae 3 and 4). Therefore, this section uses the Pearson correlation coefficient to measure the linear correlation between turbulence parameters and atmospheric stability, and the linear correlation between turbulence parameters and turbulence intensity, with the significance tested with a two-sided test. When the two-sided p-value is less than 0.05, it is considered to have passed the significance test with a 95% confidence interval. Otherwise, it is deemed to have failed the significance test. The results are shown in Figure 6.

Figure 6a is a filled contour plot of the correlation coefficients of ϵ and N in each month and at each height. Figure 6b shows the correlation coefficients of ϵ and N as well as σ_t^2 and the probability of $Ri < 0.25$ in each month and at each height. ϵ and N have an apparent positive correlation below 14 km (consistent with the conclusion of Section 4.1), and the correlation coefficient is about 0.5–0.9. However, the correlation between ϵ and N did not pass the significance test in the range of 14–17 km. ϵ and σ_t^2 have a noticeable positive correlation in the 2–18 km range, and the correlation coefficient is greater than 0.5. ϵ and the monthly frequency of $Ri < 0.25$ have a significant negative correlation in the height range of 10–12 km, and the correlation coefficient is between -0.7 and -0.8 . The above statistical results show that in the height ranges of 2–4 km and 9–13 km, the ϵ may be affected by the stability of the atmosphere and the intensity of turbulence. In the range of 4–9 km, the contribution of atmospheric dynamic stability to ϵ may be weak. In the range of 14–17 km, the intensity of turbulence may be the main factor affecting the ϵ .

Figure 6c presents the statistical results of the correlation coefficient between K_z and atmospheric stability and turbulence intensity at various heights. The results show that at 6–8 km and above 15 km, K_z and σ_t^2 have a significant positive correlation with a correlation coefficient between 0.7 and 0.9. However, the correlation with atmospheric stability parameters failed the significance test. In other altitude ranges, K_z mainly has a significant positive (negative) correlation with the monthly occurrence probability of $Ri < 0.25$ (N), especially from 2–4 km and 9–11 km, and the correlation coefficient is around 0.75 (-0.75). At about 14 km, the absolute values of the correlation coefficients between K_z and N , σ_t^2 and the monthly frequency of $Ri < 0.25$ are all about 0.7. The above results show that the main factor influencing K_z is the turbulence intensity at 6–8 km and above 15 km. In the lower troposphere (2–4 km) and near the tropopause (9–11 km), atmospheric stability has a more significant impact on K_z , which may be related to the sharp change in atmospheric stability within this height range. At about 14 km, the atmospheric stability and turbulence intensity significantly affect the K_z .

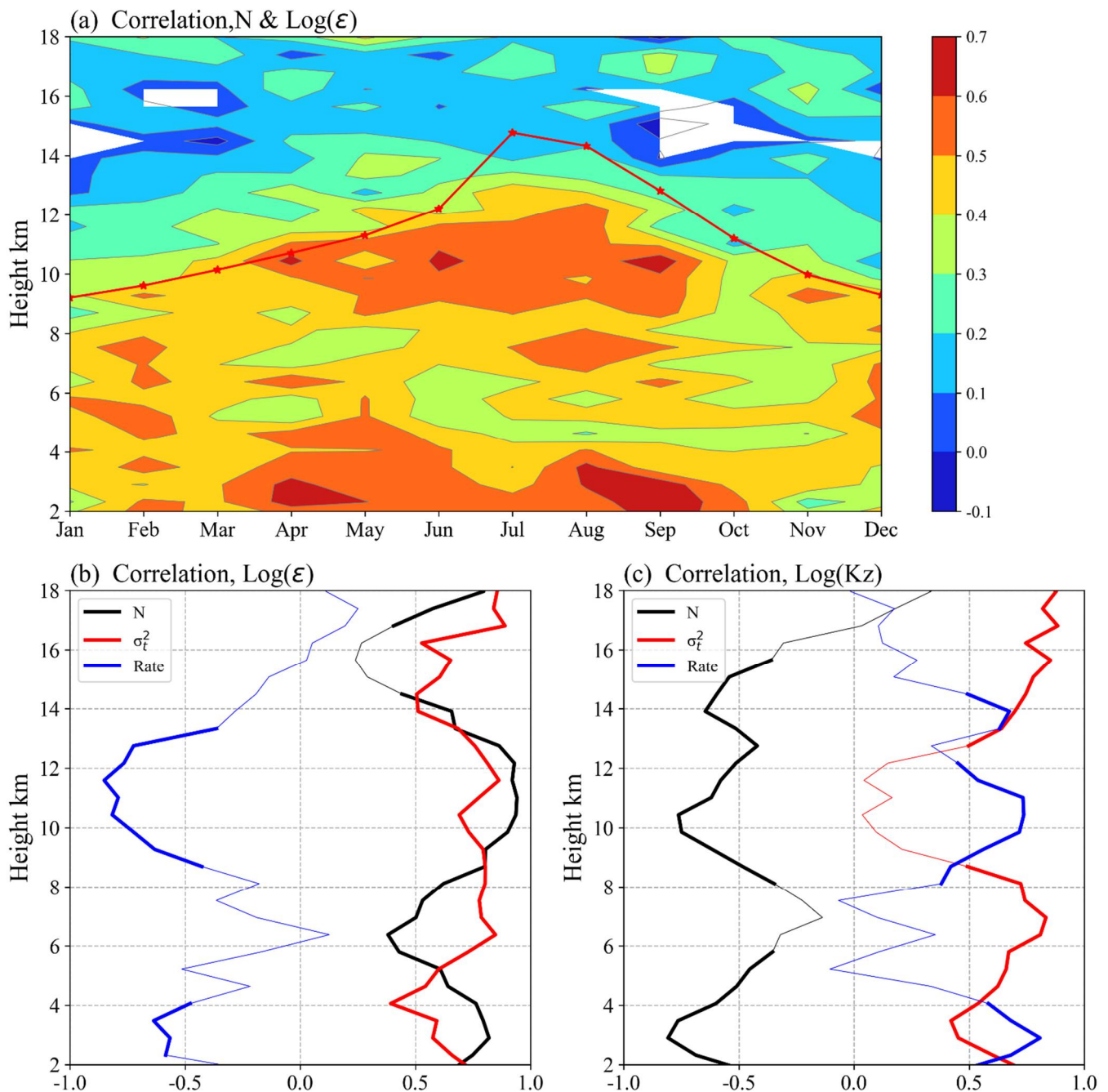


Figure 6. (a) The monthly correlation coefficient between ϵ and N in each height layer. The red dotted line is the tropopause height. (b) The correlation coefficients between ϵ and N/σ_t^2 /the frequency of $Ri < 0.25$ at various heights, represented by black/red/blue solid lines, respectively. (c) Similar to (b) but the correlation coefficients between K_z and N/σ_t^2 /the monthly frequency of $Ri < 0.25$. In (a) all monthly profile data from 2012 to 2013 are used, and in (b,c) monthly statistics are used. The blank part in (a) and the light-colored thin solid line in (b,c) indicate that the significance test with a confidence interval of 95% was not passed.

Based on the above analysis, the turbulence intensity above 15 km is the main factor affecting the ϵ and K_z . Therefore, it is vital to detect and study the stratospheric turbulence intensity. In this regard, MST radar can play an important role. The increase of turbulence intensity above 15 km may be related to gravity wave activity and its breaking, and further research should be carried out.

4.3. Increasing Rate of ϵ in the Tropopause

The results in Section 3.2 show that it is inapposite to analyze the seasonal characteristics of turbulence parameters with a simple four-season classification in Beijing. The monthly averaged profiles of ϵ show that January–May and October–December (or October to the following May) is significantly different from July and August, while June and September are transition months, as shown in Figure 7. In the height range of 6–8 km, ϵ has a minimum value and the values of ϵ change sharply from October to the following May in the range of a few kilometers above and below the height of minimum ϵ . However, the change in ϵ values at the height of the minimum-value layer is relatively gentle in July and August. At the height of about 12 km, ϵ has a maximum value from October to the following May, which is the peak value of ϵ from the tropopause to 14 km, as mentioned in Section 3.2. However, ϵ has no such maximum value in July and August.

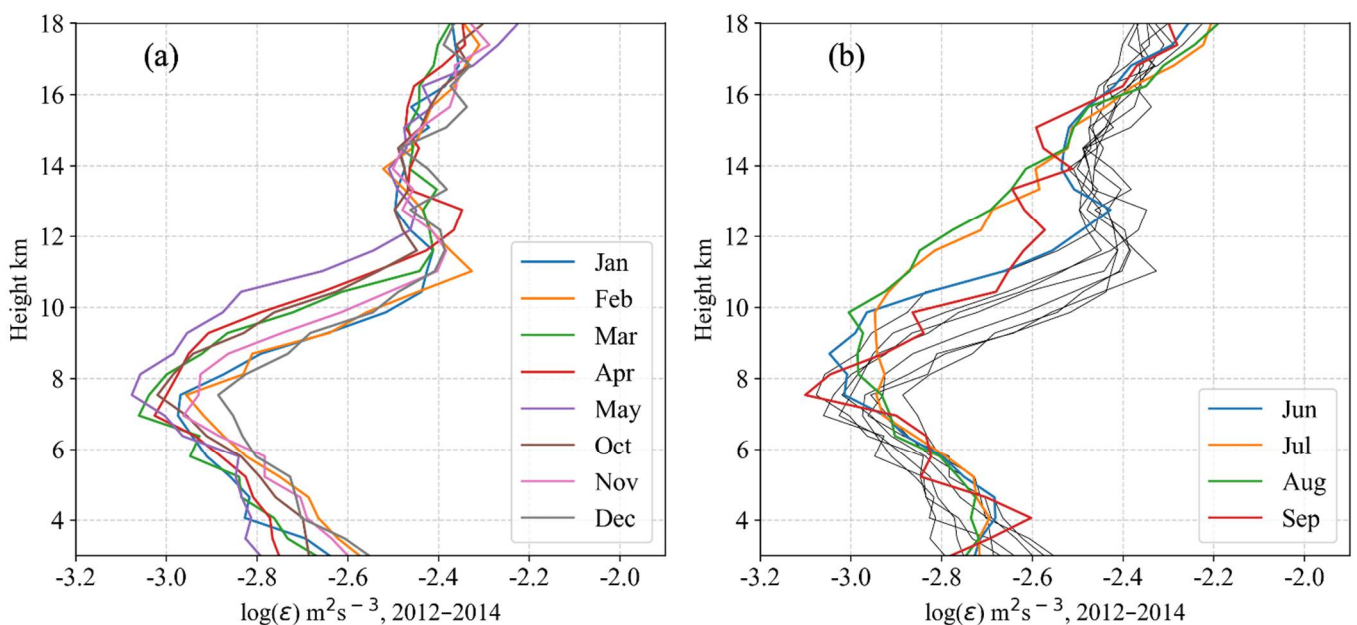


Figure 7. The monthly mean profiles of ϵ in (a) January–May and October–December, and (b) June, July–August, and September. The observational data used are from 2012–2014. The black lines are the same as (a).

In the range of 2–4 km, the profiles of ϵ have seasonal variations. From October to the following May, ϵ decreases with the same rate from 2 to 7.5 km, but tends to increase with height at 2–4 km from June to September. In the range of 6–8 km, the structure of ϵ in June is the same as in July and August, while the structure in June is the same as from October to the following May at the height of about 12 km. The structure of ϵ in September is opposite to that in June. Therefore, this study defines June and September as transition months when we discuss the seasonal variations of ϵ .

In July and August, the profiles of ϵ have no noticeable difference from 2–18 km. From October to the following May, the values of ϵ have a monthly difference in the range of 2–12 km, while the trends of the monthly mean profiles are almost the same. ϵ has a significant increase in the range of 7–11 km from October to the following May, as shown in Figure 7a. Section 3.2 also shows that ϵ has the most significant increase at the tropopause height. Some studies [13,20] have pointed out that turbulence parameters have sharp changes in the tropopause. Therefore, we reconstructed a new dataset with the reference height of the tropopause. Each profile of the new dataset varies with the height of the tropopause.

The monthly mean profiles of ϵ changing with the tropopause height are shown in Figure 8a. From October to the following May, there is no obvious monthly difference at

1 km above and below the tropopause. In the range of -1 to $+1$ km from the tropopause, the increasing linear rate of $\log(\epsilon)$ is $0.25 \text{ m}^2 \text{ s}^{-3} \text{ km}^{-1}$. The linear rate is calculated by linear regression using all scatter points in the range of -1 to $+1$ km from the tropopause, and the frequency distribution of the points is shown in Figure 8b. The red curve in Figure 8b is the mean value of ϵ at each height, and the profiles of ϵ in each month (Figure 8a) are also obtained by analyzing the frequency distribution. There are two reasons for using the average value here. First, the height of the tropopause is calculated using a sounding temperature profile with a resolution of 50 m. Therefore, the height of each profile in the new dataset is different. The new datasets need to be interpolated when analyzing the statistical characteristics of the turbulent parameters. Given that, it is more appropriate to use the monthly averaged profiles. Second, the amount of data for three years is enough to ensure that the average results can represent the statistical characteristics of turbulence parameters.

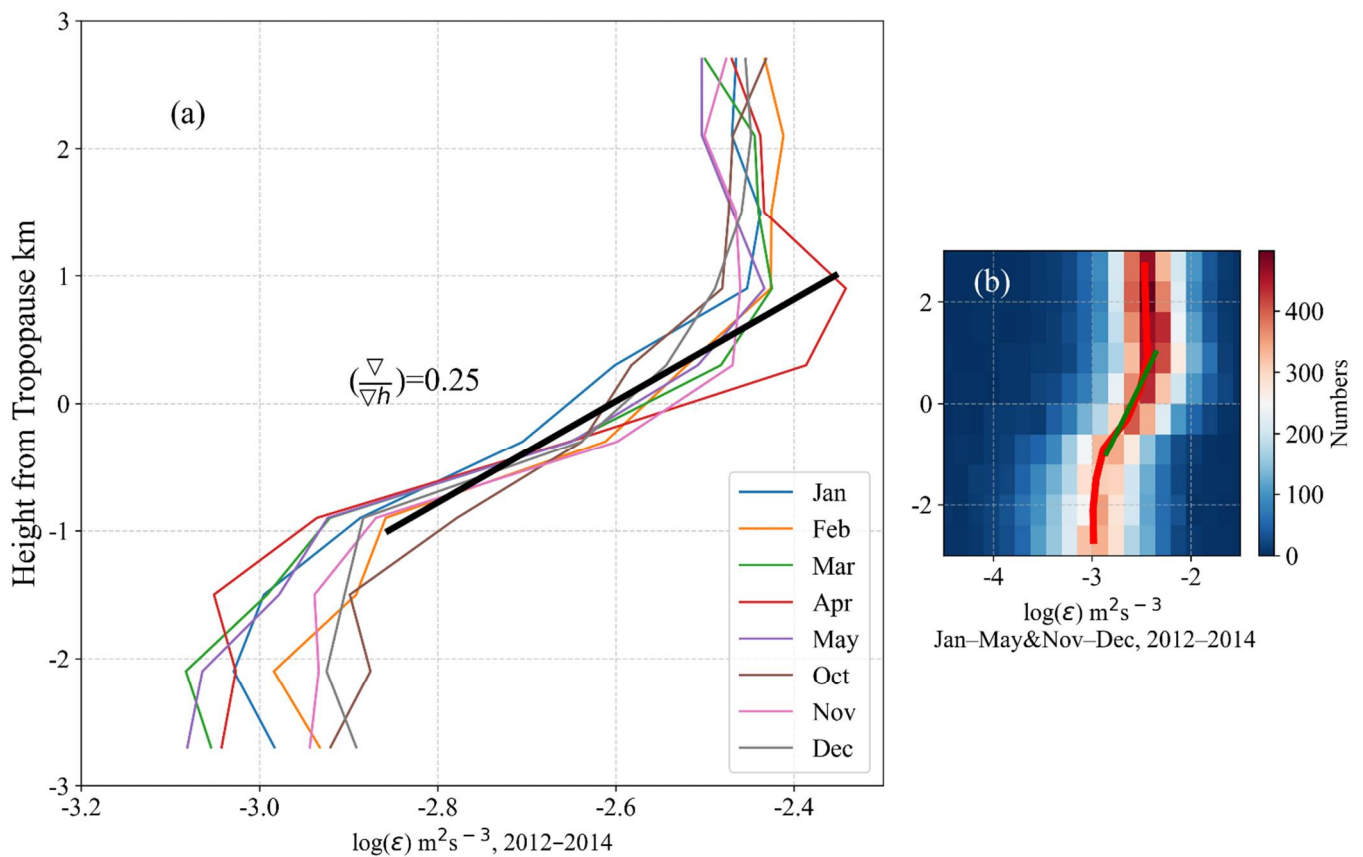


Figure 8. (a) Profiles of ϵ changing with height from the tropopause from October to the following May. (b) Frequency distribution of ϵ in the range of -3 to 3 km from the tropopause. The data used are from January to May and October to December, 2012–2014. The black solid line in (a) is the same as the green solid line in (b).

From October to the following May, in the height regions about 1 km above and below the tropopause, there is no significant difference in the profile of ϵ with the height from the tropopause, except in April, when the values of ϵ in the 0 to $+1$ km layer above the tropopause are stronger. Therefore, the tropopause is a significant reference height for studying turbulence parameters. The trend and rate of change of ϵ with height from the ground are the same in these months. Therefore, if the height of the tropopause is known, it would be likely that the monthly average profile of turbulence parameters changing with height from the ground can be obtained. However, whether this feature can be applied in specific cases requires further verification through a large number of cases.

5. Conclusions

This study used three years of data observed by Beijing's MST radar from 2012 to 2014 to calculate the turbulent parameters (ε and K_z , mainly) in the troposphere–lower stratosphere by using the spectral width method. This paper presents the characteristics of turbulence parameters changing with height in each month and season; plus, comparison of the seasonal variations between turbulence parameters and atmospheric stability (N and Ri) was also conducted. The conclusions are as follows:

1. The ε in Beijing is distributed from 10^{-4} to $10^{-1.5}$ $\text{m}^2 \text{s}^{-3}$, spanning 2.5 orders of magnitude, and the shape conforms to the Gaussian distribution. The median values of ε are from 10^{-3} to $10^{-2.5}$ $\text{m}^2 \text{s}^{-3}$. K_z is distributed between 10^0 and 10^1 $\text{m}^2 \text{s}^{-1}$, spanning an order of magnitude. The median values of K_z are distributed between $10^{0.4}$ and $10^{0.75}$ $\text{m}^2 \text{s}^{-1}$. The turbulence parameters of Beijing MST radar show inconsistency with some of the results of previous studies, but are more consistent with the results of Harrow radar (42.04°N , 82.89°W) which is located at the nearest latitude compared with the Beijing MST radar site [13].
2. Comparison of turbulence parameters and the monthly variation characteristics of atmospheric stability with altitude showed that the vertical structure of N and ε in the height range of 2–18 km has good consistency. In the range of 2–14 km, the Pearson correlation coefficient is between 0.5 and 0.9. From the tropopause to 14 km in Beijing, the values of ε and N both have a peak layer from October to the following May.
3. The frequency of $\text{Ri} < 0.25$ is in good agreement with the vertical structure of K_z in the region below the tropopause. Within the height range of 2–4 km from the ground in Beijing, K_z and the percentage of $\text{Ri} < 0.25$ have a significant correlation, with a Pearson correlation coefficient of about 0.75, and both have a large-value layer in March–May and September–October.

It is worth noting that the results of this study show that not only are the seasonal divisions of different regions different, but the seasonal divisions of different atmospheric layers in the same region are also different. The statistical results of ε indicate that June and September are the transition months in Beijing, and the vertical structure of ε is one type from October to the following May, and another type in July and August. However, the statistical results of K_z show that this seasonal classification is unsuitable in the height range of 2–4 km, while this seasonal classification is suitable for K_z at heights above 4 km. The seasonal variation of the vertical structure of K_z is more complex, which indicates that there are specific differences in the beginning and end months of different seasons at different levels of the atmosphere.

This paper gives the statistical results of turbulence parameters, but how the turbulence parameters change during synoptic processes needs to be further investigated. For example, the correlation analysis in this paper shows that the turbulence parameters above 15 km may be mainly affected by the turbulence intensity; the results of Khoma et al. [15] show that the seasonal characteristics of turbulence parameters are related to gravity waves in the Antarctic stratosphere; and Li et al. [14] calculated ε under different Ri, and the results showed that the median values of ε when $\text{Ri} < 1$ is 3.2 times that of when $\text{Ri} > 1$. From October to the following May, in the height layer of 1 km above and below the tropopause, there is no apparent seasonal difference in the monthly average profile of ε . Additionally, $\log(\varepsilon)$ increases sharply with a rate of $0.25 \text{ m}^2 \text{ s}^{-3} \text{ km}^{-1}$, derived by linear regression. This vertical structure of ε indicates that the tropopause is a suitable reference height for studying turbulence parameters. Although some studies have used the tropopause as the reference height to analyze the statistical characteristics of turbulence parameters [20], [13], a large number of case studies are still needed to discuss the role of the tropopause in studying the vertical structure of turbulence parameters.

Author Contributions: Conceptualization, Y.T. and Z.C.; methodology, Z.C.; software, Z.C.; validation, Z.C., Y.T. and D.L.; formal analysis, Z.C., Y.T. and D.L.; investigation, Z.C. and Y.T.; writing—original draft preparation, Z.C.; writing—review and editing, Z.C., Y.T. and D.L.; visualization, Z.C. All authors have read and agreed to the published version of the manuscript.

Funding: This research was funded by the National Natural Science Foundation of China (Grant No. 41905042, 41861134034). This work was supported by the Open Research Project of Large Research Infrastructures of CAS- “Study on the interaction between low/mid-latitude atmosphere and ionosphere based on the Chinese Meridian Project” and the Key Research Project of Frontier Science of Chinese Academy of Sciences (QYZDY-SSW-DQC027).

Institutional Review Board Statement: Not applicable.

Informed Consent Statement: Not applicable.

Data Availability Statement: Data related to this article are available upon request to the corresponding authors.

Acknowledgments: We acknowledge the use of data from the Chinese Meridian Project. We sincerely thank all the referees and the editors for their constructive comments and suggestions.

Conflicts of Interest: The authors declare no conflict of interest.

References

1. Lilly, K.; Waco, E.; Adelfang, I. Stratospheric Mixing Estimated from High-Altitude Turbulence Measurements. *J. Appl. Meteorol.* **1974**, *13*, 488–493. [[CrossRef](#)]
2. Weinstock, J. Using radar to estimate dissipation rates in thin layers of turbulence. *Radio Sci.* **1981**, *16*, 1401–1406. [[CrossRef](#)]
3. Hocking, W.K. On the extraction of atmospheric turbulence parameters from radar backscatter Doppler spectra—I. Theory. *J. Atmos. Terr. Phys.* **1983**, *45*, 89–102. [[CrossRef](#)]
4. Hocking, W.K. Measurement of turbulent energy-dissipation rates in the middle atmosphere by radar techniques—A review. *Radio Sci.* **1985**, *20*, 1403–1422. [[CrossRef](#)]
5. Batchelor, G.K. *The Theory of Homogeneous Turbulence*; Cambridge University Press: Cambridge, UK, 1953.
6. Tatarski, V.I. *Wave Propagation in a Turbulent Medium*; Courier Dover Publications: Mineola, NY, USA, 1961.
7. Nastrom, G.D. Doppler radar spectral width broadening due to beamwidth and wind shear. *Ann. Geophys. Atmos. Hydrospheres Space Sci.* **1997**, *15*, 786–796. [[CrossRef](#)]
8. Dehghan, A.; Hocking, W.K. Instrumental errors in spectral-width turbulence measurements by radars. *J. Atmos. Sol. Terr. Phys.* **2011**, *73*, 1052–1068. [[CrossRef](#)]
9. Satheesan, K.; Murthy, B.V.K. Turbulence parameters in the tropical troposphere and lower stratosphere. *J. Geophys. Res. Atmos.* **2002**, *107*, ACL-2. [[CrossRef](#)]
10. Thorpe, S.A. Turbulence and Mixing in a Scottish Loch. *Philos. Trans. R. Soc. Lond.* **1977**, *286*, 125–181.
11. Zink, F.; Vincent, R.A.; Murphy, E.; Cote, O. Comparison of radar and in situ measurements of atmospheric turbulence. *J. Geophys. Res. Atmos.* **2004**, *109*, D11108. [[CrossRef](#)]
12. Li, Q.; Rapp, M.; Schroen, A.; Schneider, A.; Stober, G. Derivation of turbulent energy dissipation rate with the Middle Atmosphere Alomar Radar System (MAARSY) and radiosondes at Andoya, Norway. *Ann. Geophys.* **2016**, *34*, 1209–1229. [[CrossRef](#)]
13. Kohma, M.; Sato, K.; Tomikawa, Y.; Nishimura, K.; Sato, T. Estimate of Turbulent Energy Dissipation Rate from the VHF Radar and Radiosonde Observations in the Antarctic. *J. Geophys. Res. Atmos.* **2019**, *124*, 2976–2993. [[CrossRef](#)]
14. Jaiswal, A.; Phanikumar, D.V.; Bhattacharjee, S.; Naja, M. Estimation of Turbulence Parameters Using ARIES ST Radar and GPS Radiosonde Measurements: First Results from the Central Himalayan Region. *Radio Sci.* **2020**, *55*, 1–18. [[CrossRef](#)]
15. Kantha, L.; Hocking, W. Dissipation rates of turbulence kinetic energy in the free atmosphere: MST radar and radiosondes. *J. Atmos. Sol. Terr. Phys.* **2011**, *73*, 1043–1051. [[CrossRef](#)]
16. Fukao, S.; Yamanaka, M.D.; Ao, N.; Hocking, W.K.; Sato, T.; Yamamoto, M.; Nakamura, T.; Tsuda, T.; Kato, S. Seasonal variability of vertical eddy diffusivity in the middle atmosphere: 1. Three-year observations by the Middle and Upper-atmosphere radar. *J. Geophys. Res. Atmos.* **1994**, *99*, 18973–18987. [[CrossRef](#)]
17. Yamanaka, M.D.; Kurosaki, S.; Fukao, S.; Hashiguchi, H.; Tsuda, T.; Kato, S. Seasonal and interannual variabilities of vertical eddy diffusivity observed by the MU-Radar. *Adv. Space Res.* **1994**, *14*, 277–280. [[CrossRef](#)]
18. Kurosaki, S.; Yamanaka, M.D.; Hashiguchi, H.; Sato, T.; Fukao, S. Vertical eddy diffusivity in the lower and middle atmosphere: A climatology based on the MU radar observations during 1986–1992. *J. Atmos. Terr. Phys.* **1996**, *58*, 727–734. [[CrossRef](#)]
19. Nastrom, G.D.; Eaton, F.D. Seasonal variability of turbulence parameters at 2 to 21 km from MST radar measurements at Vandenberg Air Force Base, California. *J. Geophys. Res. Atmos.* **2005**, *110*, D19110. [[CrossRef](#)]
20. Nastrom, G.D.; Eaton, F.D. Turbulence eddy dissipation rates from radar observations at 5–20 km at White Sands Missile Range, New Mexico. *J. Geophys. Res. Atmos.* **1997**, *102*, 19495–19505. [[CrossRef](#)]

21. Nastrom, G.D.; Eaton, F.D. A brief climatology of eddy diffusivities over White Sands Missile Range, New Mexico. *J. Geophys. Res. Atmos.* **1997**, *102*, 29819–29826. [[CrossRef](#)]
22. Rao, D.N.; Ratnam, M.V.; Rao, T.N.; Rao, S.V.B. Seasonal variation of vertical eddy diffusivity in the troposphere, lower stratosphere and mesosphere over a tropical station. *Ann. Geophys.* **2001**, *19*, 975–984. [[CrossRef](#)]
23. Rao, D.N.; Rao, T.N.; Venkataratnam, M.; Thulasiraman, S.; Rao, S.V.B.; Srinivasulu, P.; Rao, P.B. Diurnal and seasonal variability of turbulence parameters observed with Indian mesosphere-stratosphere-troposphere radar. *Radio Sci.* **2001**, *36*, 1439–1457. [[CrossRef](#)]
24. Rao, D.N.; Kishore, P.; Rao, T.N.; Rao, S.V.B.; Reddy, K.K.; Yarraiah, M.; Hareesh, M. Studies on refractivity structure constant, eddy dissipation rate, and momentum flux at a tropical latitude. *Radio Sci.* **1997**, *32*, 1375–1389. [[CrossRef](#)]
25. Singh, N.; Joshi, R.R.; Chun, H.Y.; Pant, G.B.; Damle, S.H.; Vashishtha, R.D. Seasonal, annual and inter-annual features of turbulence parameters over the tropical station Pune (18°32' N, 73°51' E) observed with UHF wind profiler. *Ann. Geophys.* **2008**, *26*, 3677–3692. [[CrossRef](#)]
26. Tian, Y.; Lü, D. Preliminary analysis of Beijing MST radar observation results in the mesosphere-lower thermosphere. *Chin. J. Geophys.* **2016**, *59*, 440–452. (In Chinese) [[CrossRef](#)]
27. Tian, Y.; Lü, D. Comparison of Beijing MST radar and radiosonde horizontal wind measurements. *Adv. Atmos. Sci.* **2017**, *34*, 39–53. [[CrossRef](#)]
28. Chen, Z.; Tian, Y.; Lü, D. Improving the processing algorithm of Beijing MST radar power spectral density data. *J. Appl. Meteor. Sci.* **2020**, *31*, 694–705. [[CrossRef](#)]
29. Kantha, L.; Lawrence, D.; Luce, H.; Hashiguchi, H.; Tsuda, T.; Wilson, R.; Mixa, T.; Yabuki, M. Shigaraki UAV-Radar Experiment (ShUREX): Overview of the campaign with some preliminary results. *Prog. Earth Planet Sci.* **2017**, *4*, 1–26. [[CrossRef](#)]
30. Tsuda, T.; Sato, T.; Hirose, K.; Fukao, S.; Kato, S. MU radar observations of the aspect sensitivity of backscattered VHF echo power in the troposphere and lower stratosphere. *Radio Sci.* **1986**, *21*, 971–980. [[CrossRef](#)]